Construction and Building Materials 505 (2025) 144807

Contents lists available at ScienceDirect

Construction and Building Materials

journal homepage: www.elsevier.com/locate/conbuildmat

Particle-size sensors of different geometry to assess the workability of asphalt mixtures

Omar Guazzaroni, Lorenzo Paolo Ingrassia *, Amedeo Virgili, Andrea Graziani, Francesco Canestrari

Università Politecnica delle Marche, Via Brecce Bianche, Ancona 60131, Italy

ARTICLE INFO

Keywords:
Particle-size sensor
Asphalt mixture
Workability
Compaction
Relative Rotation
Relative Rotation Capacity
Average Residual Rotation
Gyratory Compactor

ABSTRACT

The compaction process of asphalt mixtures has a great influence on the durability and long-term performance of flexible pavements. To improve the field compaction process, particle-size sensors have recently been introduced and standardised to assess the workability of asphalt mixtures. Most studies employ cubic shell sensors or sensors with an irregular shape. Moreover, to date, no study has assessed whether the choice of the gyratory compactor can affect the sensor measurements. Within this context, the objective of this study is to compare particle-size sensors with easily reproducible shell geometries (cubic, spherical), in order to verify their behaviour during compaction and their ability to assess the workability of three asphalt mixtures with different characteristics. Moreover, the study compares two gyratory compactors with different compaction mechanisms to provide a preliminary analysis of the gyratory compactor influence. The results indicate that the spherical sensor can be more sensitive to workability variations. Furthermore, the cubic sensor may hinder compaction in the surrounding area by impeding the movement of the adjacent aggregates. The compaction mechanism, which can vary for different gyratory compactors, may have a certain influence on the compaction process. Finally, the ratio between the sensor size and the mixture nominal maximum aggregate size is an aspect to be taken into due consideration.

1. Introduction

The compaction process of asphalt mixtures represents a critical phase in the construction of road pavements. Ensuring proper compaction is essential to achieve durability and long-term performance. Several compaction methods are used in the laboratory to study the densification process, such as the gyratory compactor, the roller compactor, the static compactor, and the Marshall impact compactor [1,2]. However, the final properties of the mixture, although ideally governed solely by its composition and volumetrics, are in practice strongly affected by the compaction method and conditions, making the densification process particularly complex to analyse [3]. Consequently, open issues remain regarding the correlation between the compaction behaviour evaluated in the laboratory and that observed in the field. This is the reason why the compaction process in the field is still mostly based on practical experience, which often leads to pavement performance issues in the long-term.

For these reasons, particle-size sensors have been recently introduced in pavement engineering to investigate the workability of asphalt mixtures. These sensors typically consist of an external shell of thermoplastic polymer and an internal wireless sensor that can measure accelerations, rotations and temperature. The collected data is then transmitted in real time to a digital device via Bluetooth technology. This type of sensor was introduced in civil engineering to investigate the movement of railway ballast particles [4,5]. In these first applications, an external shell similar to a real ballast particle with a nominal size of 60 mm was used. The size of the sensors was then reduced to be implemented in asphalt mixture research. This innovative technology was initially used to investigate the kinematics of coarse aggregate particles during the gyratory compaction in the laboratory [3]. Since the sensors proved to be effective in investigating the compaction behaviour of asphalt mixtures, their use in pavement engineering has been recently standardised by ASTM D8541 [6]. A review of the literature shows that particle-size sensors with different geometries and nominal sizes have

* Corresponding author.
E-mail addresses: o.guazzaroni@pm.univpm.it (O. Guazzaroni), l.p.ingrassia@pm.univpm.it (L.P. Ingrassia), a.virgili@univpm.it (A. Virgili), a.graziani@univpm.it (A. Graziani), f.canestrari@univpm.it (F. Canestrari).

https://doi.org/10.1016/j.conbuildmat.2025.144807
Received 25 July 2025; Received in revised form 12 November 2025; Accepted 5 December 2025
Available online 9 December 2025

Table 1
Relevant literature concerning the use of particle-size sensors in laboratory experiments with the gyratory compactor (150 mm diameter mould).

Sensor external geometry	Sensor nominal size [mm]	Mixture NMAS [mm]	Sensor nominal size / NMAS [-]	Reference
Cubic	23	20	1.15	[25]
	25	26.5	0.94	[15]
	26	25 – 20 – 16	1.04 – 1.625	[7]
	27	12.5	2.16	[8] [14]
		12.5 – 9.5	2.16 – 2.84	[19]
		20	1.35	[9] [11]
		26.5	1.02	[12]
Parallelepiped	Not declared	13	Not computable	[22] [26]
Irregular shape	Not declared	9.5	Not computable	[3]
		12.5–9.5	Not computable	[24]
		12.5	Not computable	[32]
		26.5	Not computable	[13]

Table 2
Characteristics of the studied asphalt mixtures.

Mixture	Binder	Binder [%]	RAP [%]	NMAS [mm]
Wearing	50/70 pen	5.8	-	6.3
Binder	50/70 pen	4.7	-	16
Base	PMB (3.8 % SBS)	4.3	30	20

Note: PMB = polymer-modified bitumen; SBS = styrene-butadiene-styrene polymer

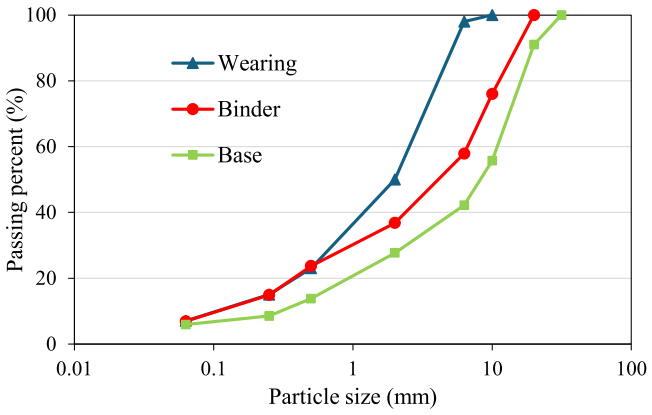

Fig. 1. Gradation curve of the studied asphalt mixtures.

been used in laboratory experiments with the gyratory compactor. Table 1 summarises the relevant references involving a 150 mm diameter mould and reports, for each study, the mixture nominal maximum aggregate size (NMAS) and the ratio between sensor size and NMAS.

Particle-size sensors allow assessing several variables during the compaction process. In fact, they were used to demonstrate that aggregate size and gradation affect the compaction behaviour [7] and to study the effects of compaction temperature and Warm Mix Asphalt additives on workability [8,9]. Moreover, this technology was also tested for other pavement materials, such as unbound aggregate for base layers [10,11] and cold recycled mixtures [12].

Particle-size sensors have also been used to evaluate aggregate particle motion under the action of different rollers during field compaction [13,14], highlighting that the acceleration induced by vibrating drums is the main parameter affecting the compaction process [15–17].

Other studies have explored applications other than the evaluation of compaction. For example, particle-size sensors could allow to estimate the stiffness modulus of asphalt layers in the context of structural health monitoring [18,19]. In addition, the sensor data also show potential in detecting pavement distresses such as rutting, cracking and water damage [20]. Moreover, particle-size sensors proved to sense stress changes within cementitious mixtures, thus representing a useful tool for assessing the different stages of strength evolution and damage development for this type of materials [21].

To better understand the compaction phenomenon, recent studies simulated Marshall and gyratory compaction with the discrete element method and calibrated the model by using particle-size sensor data [22]. Moreover, advanced computer modelling methods such as Bullet physics engine [23] and Machine Learning [24] have been combined with the use of particle-size sensors to predict the compaction conditions of asphalt pavements.

The literature analysis presented above reveals the potential of using particle-size sensors for the compaction quality control of asphalt pavements, as they allow real-time estimation of the compaction degree and are generally easier to install and more efficient than conventional sensors.

However, it has recently been shown that particle contact stresses are influenced by the aggregate shape [25] and that the dimension of the particle-size sensor affects the meso-structural properties of asphalt mixtures [26]. Furthermore, as shown in Table 1, most studies employed cubic shell sensors, while others used sensors with an irregular external geometry, intended to reproduce real aggregates. A cubic sensor, due to its flat surfaces, may rotate with greater difficulty during compaction than the irregular one, while irregular sensors raise reproducibility issues because their geometry is not consistently defined. In addition, the studies available in the literature used different gyratory compactors without, however, verifying whether the compactor itself is a variable affecting the sensor measurements.

Within this context, the objective of this study is to compare particle-size sensors of different geometry, in order to verify their behaviour during compaction and their ability to analyse the compaction process. To this aim, two easily reproducible shell geometries (cubic, spherical) and three asphalt mixtures with different characteristics (e.g., NMAS) are investigated in the laboratory. Moreover, the study compares two gyratory compactors with different compaction mechanisms, in order to provide a preliminary analysis of the gyratory compactor influence.

2. Materials and methods

2.1. Asphalt mixtures

The experimental program considered three dense-graded asphalt concrete mixtures for different pavement layers, i.e., for wearing, binder and base courses, all produced at the asphalt plant. They were chosen specifically for their distinct characteristics in terms of aggregate gradation, NMAS, binder type and dosage, and reclaimed asphalt pavement (RAP) content (Table 2, Fig. 1). The investigated wearing course mixture is mainly used for microsurfacings.

2.2. Compaction

The gyratory compaction was carried out by the simultaneous action of static compression and shear stresses, by considering the standard test conditions specified by EN 12697–31 [27]: gyration angle of 1.25°, rotation speed of 30 rpm, vertical pressure of 600 kPa. Two gyratory compactors, characterized by different compaction mechanisms, were considered. The main difference between them is the movement of the mould during the compaction process.

Gyratory compactor 1 (Fig. 2(a)), model GYROCOMP by IPC GLOBAL, is characterized by the rotation of the entire system (mould, specimen and loading plates) around its inclined axis. According to the manufacturer, this compactor provides accurate and repeatable test results, together with stiffness and angular stability values within the

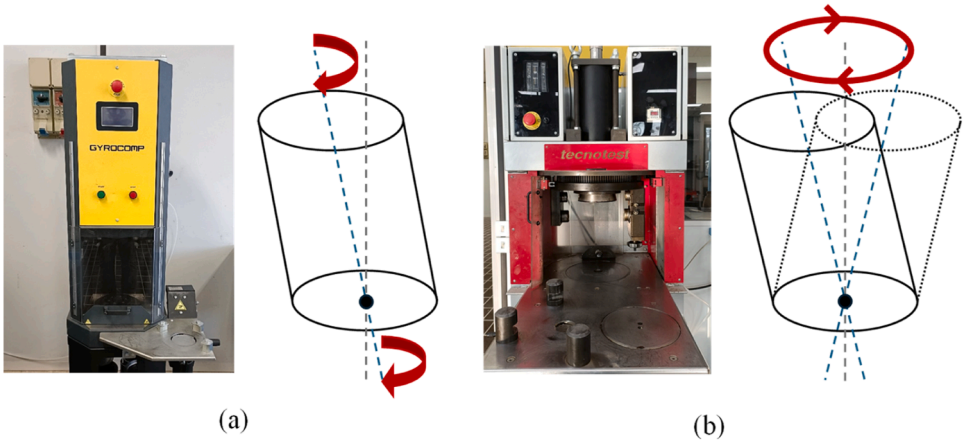

Fig. 2. Gyratory compactors: (a) Compactor 1, (b) Compactor 2.

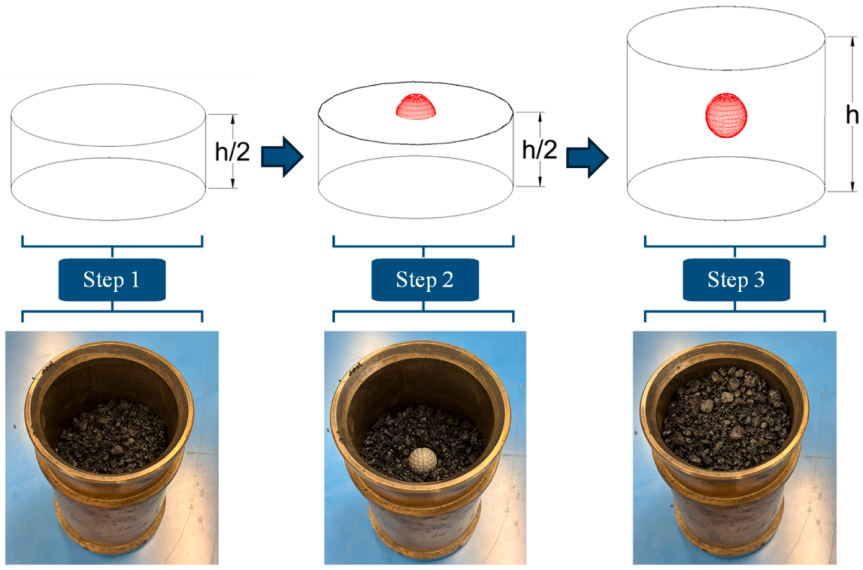

Fig. 3. Specimen preparation steps.

Table 3
Experimental program.

Mixture	Compactor 1		Compactor 2
	Cubic shell	Spherical shell	Cubic shell
Wearing	×	×	
Binder	×	×	×
Base	×	×	

limits defined by EN 12697–31 [27]. The manufacturer also states that this mechanism is completely equivalent to the mechanism of Compactor 2 described below.

Gyratory compactor 2 (Fig. 2(b)), model B100B92 by TECNOTEST, follows the exact compaction principle described in the standard EN 12697–31 [27]. Compaction is induced through a rigid circular motion of the top surface of the mould, which generates a conical surface of revolution (considering the specimen axis). During this process, the top and bottom surfaces of the specimen remain perpendicular to the axis of the conical surface.

One of the objectives of this study is to check the equivalence between these two compaction mechanisms by analysing the particle motion characteristics measured by particle-size sensors.

The asphalt mixtures were sampled at the asphalt plant and reheated in the oven (model M250-VF by MPM Instruments) at 160 °C ± 1.5 °C for three hours to prepare specimens with a diameter of 150 mm and a mass of approximately 4800 g. The specimen preparation took approximately one minute and consisted of three steps (Fig. 3): placing half of the material in the mould (also heated at 160 °C ± 1.5 °C for three hours) trying to obtain a horizontal surface; placing the particle-size sensor in the centre (following recommendations from previous studies [3,7] and from the reference standard [6]); and pouring the remaining material in the mould. The filled mould was then placed in the gyratory compactor and compaction was initiated within one minute. The same procedure was followed for both shells (cubic, spherical). As a first attempt, to prevent any damage to the shells, the number of test gyrations was limited to 80.

The two sensors were tested in combination with all asphalt mixtures using Compactor 1. Instead, the effect of the gyratory compactor mechanism was evaluated with the cubic sensor for the binder mixture. The experimental program is summarized in Table 3. For each combination reported in the table, two replicate specimens were compacted.

2.3. Particle-size sensors and workability parameters

The employed particle-size sensors are composed by an external shell

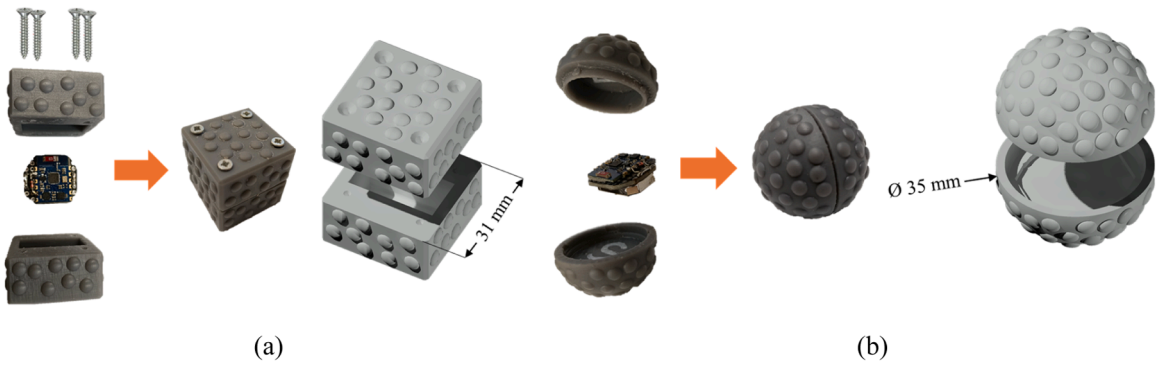

Fig. 4. Particle-size sensors: (a) cubic shell, (b) spherical shell.

Table 4
Post-curing characteristics of the resin used for the external shells.

Property	Value
Ultimate tensile strength [MPa]	65
Tensile modulus [GPa]	2.8
Flexural modulus [GPa]	2.2
Impact resistance (notched Izod test) [J/m]	25
Elongation at break [%]	6
Heat deflection temperature at 1.8 MPa [°C]	58
Heat deflection temperature at 0.45 MPa [°C]	73

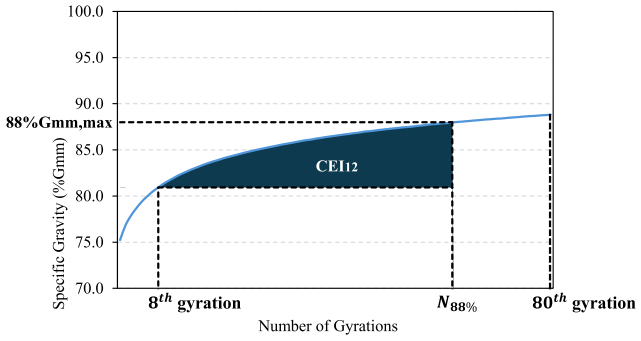

Fig. 5. Definition of the Compaction Energy Index "CEI_{12}".

made of resin and an internal wireless sensor that integrates the MPU9250 micro electro-mechanical systems (MEMS) sensor. This sensor comprises a three-axis accelerometer, a three-axis gyroscope and a three-axis magnetometer. The module comes with pre-installed firmware allowing communication with a smartphone via Bluetooth. To ensure greater stability and ease of use, the module was installed on a custom-designed printed circuit board (PCB). Given the low energy consumption of the internal sensor, it is powered by a common CR2032 lithium primary cell.

The effect of the shell shape was investigated using two types of shells, cubic and spherical (Fig. 4). These shells were made of a selected resin and produced through stereolithography (SLA) 3D printing technology. Temperature and stress resistances during compaction are ensured by the post-curing characteristics of the chosen resin (Table 4). Both shell types are reusable and ensure adequate Bluetooth communication between sensor and smartphone. They were designed to replicate the size and behaviour of a coarse aggregate within the asphalt mixture, compatibly with the internal sensor hardware dimension. For this reason, the cubic shell features a side length of 31 mm, whereas the spherical one has a diameter of 35 mm. To enhance interlocking during the compaction process, spherical caps with a base radius of 2.2 mm and a height of 1 mm were randomly placed on the external surfaces of the shells. The difference in dimensions between the two shells is due to the need to maintain a minimum external thickness to meet mechanical requirements [28].

The ratio between sensor size and NMAS were 1.55, 1.94 and 4.92 for the cubic sensor and 1.75, 2.19 and 5.55 for the spherical sensor. The lowest and intermediate values correspond to the mixtures with NMAS of 20 and 16 mm and are consistent with those previously investigated in the literature (Table 1). The highest values correspond to the mixture with NMAS of 6.3 mm and may be useful for evaluating the effect of the ratio between sensor size and mixture NMAS.

Before starting all tests, the sensor auto-calibration procedure is performed, which aligns the z-axis of the local coordinate system (perpendicular to the plane of the PCB) with the direction of the acceleration of gravity (global coordinate Z). During compaction, the particle-size sensor records accelerations, Euler angles, angular velocities, and magnetic field data at a sampling rate of 10 Hz. The acquired Euler angles are expressed in the local coordinate system of the sensor (previously aligned to the global system through the auto-calibration procedure).

In the few seconds between the auto-calibration and the start of rotation, the sensor may move due to minor material rearrangement. For this reason, during post-processing, the Euler angles are re-transformed into the global coordinate system, as required by the ASTM D8541 standard. This transformation is performed using quaternion-based rotation matrices derived from the initial quaternion data collected in the first six seconds, before the start of compaction.

To reduce noise and remove signal trend, the global Euler angle data collected during compaction are smoothed using a third-order Fourier polynomial. The fitted signals are then used to compute the Relative Rotation (RR), as defined in ASTM D8541 [6], which corresponds to the difference between the maximum and minimum values of each global Euler angle within a single compaction cycle.

The Relative Rotation Capacity (RRC) is then defined as the area under the RR curve from N_i to N_d:

$$\mathrm{RRC} = \sum_{i=N_i}^{N_d} \frac{(RR_{i+1} + RR_i) \bullet l}{2} \quad (1)$$

where N_i denotes the initial number of gyrations; N_d is the design number of gyrations; RR_i and RR_{i+1} represent the relative rotations at the i^{th} and $(i+1)^{th}$ gyration, respectively; l refers to the length of the x-axis unit (one compaction gyration). In this study, N_i was assumed equal to 8, consistently with the definition of the Compaction Energy Index (CEI) given below, whereas N_d corresponded to the total number of test gyrations (80).

The Average Residual Rotation (ARR) is calculated by comparing the relative rotations of two asphalt mixtures (test mixture versus control mixture). The residual rotation at a specific gyration cycle is the difference between the relative rotations of the two mixtures at the cor-

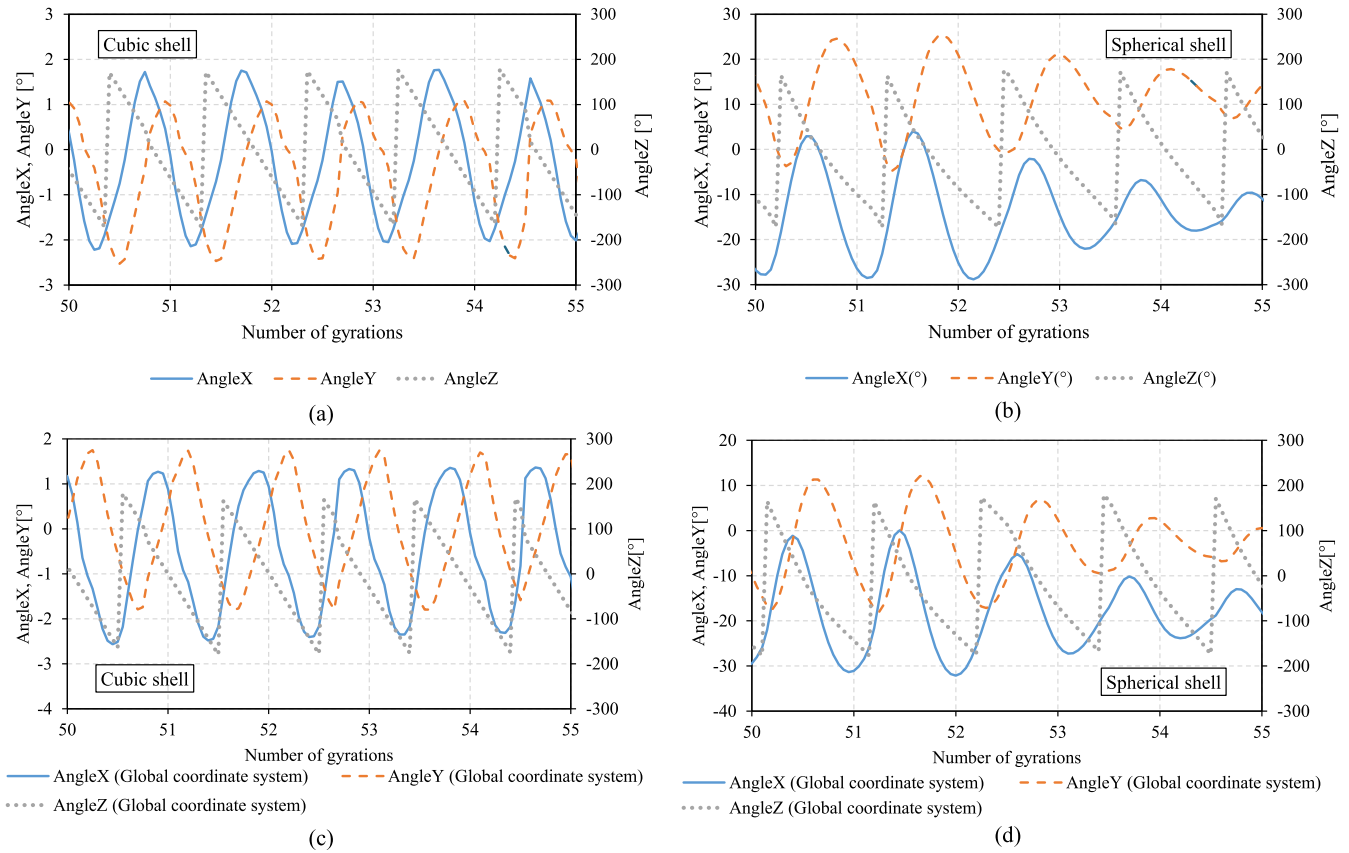

Fig. 6. Measured and global Euler angles for the binder mixture (Compactor 1): (a) cubic shell (measured), (b) spherical shell (measured), (c) cubic shell (global), (d) spherical shell (global).

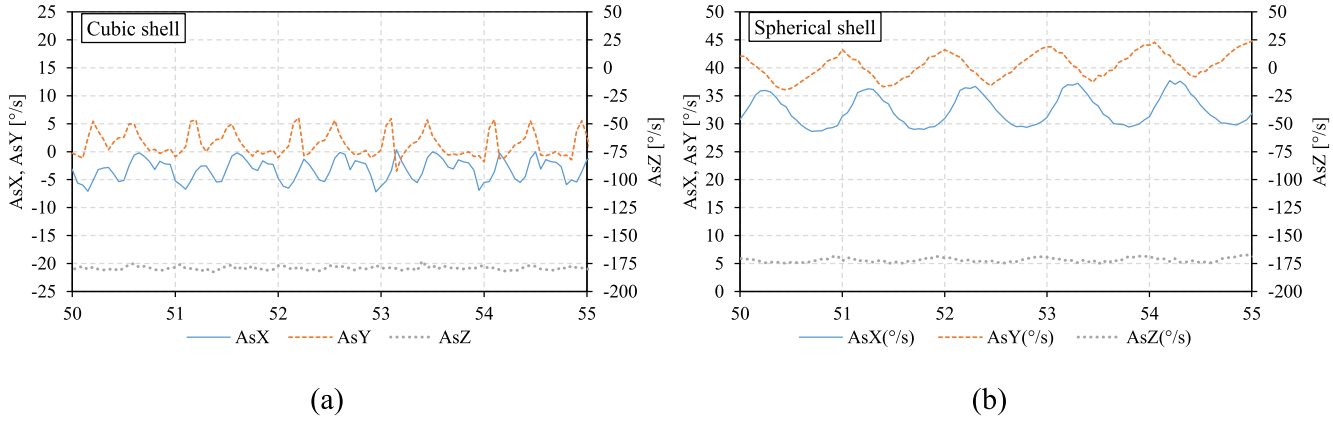

Fig. 7. Angular velocity measured with Compactor 1 for the binder mixture: (a) Cubic shell, (b) Spherical shell.

responding gyration. ARR is the average value of the residual rotation from N_i to N_d:

$$\mathrm{ARR} = \sum_{i=N_i}^{N_d} \frac{(RR_{t,i} - RR_{c,i})}{N_d - N_i} \bullet Q \tag{2}$$

where $RR_{c,i}$ and $RR_{t,i}$ are the relative rotations at the i^{th} gyration for the control mixture and for the test mixture, respectively; Q is a coefficient for improving the sensitivity of the parameter (a scaling factor of 10 is suggested for conventional asphalt mixtures [6]). A positive value of ARR indicates that the test mixture is characterized by a more active particle rotation during compaction with respect to the control mixture, i.e., better workability. Vice versa, a negative value of ARR means that the test mixture has worse workability than the control mixture.

The air void percentage of the compacted specimens (V_a) was calculated according to EN 12697–8 [29]:

$$V_a = \frac{(\rho_m - \rho_b)}{\rho_m} \bullet 100 \tag{3}$$

where ρ_m is the maximum density of the mixture and ρ_b is the bulk density of the specimen. The latter was calculated following EN 12697–6 [30] (geometric method) by subtracting the mass and the volume of the particle-size sensor:

$$\rho_b = \frac{m - m_{Sensor}}{\frac{\pi}{4} \bullet d^2 \bullet h - V_{Sensor}} \tag{4}$$

where m is the mass of the dry compacted specimen, h is the height of the compacted specimen, d is the specimen diameter (150 mm), m_{Sensor} and V_{Sensor} are the mass and the volume of the particle-size sensor, respectively. Using this method, the open voids are included in the void content calculation. However, this does not significantly affect the relative comparisons, as the same procedure was applied to all specimens.

A customized version of the well-known Compaction Energy Index (CEI) [31] was also used to better assess the workability of the asphalt mixtures. This customized index represents the area under the compaction curve from the 8th gyration until a compaction degree of 88 % is reached (Fig. 5). The 88 % compaction degree was chosen, instead of the 92 % of the original CEI definition, because it was achieved in all tests performed. As gyratory compaction curves tend to flatten at higher gyration levels, calculating the CEI using compaction degrees of 88 % or 92 % typically produces very similar results. Since this index quantifies the energy needed to achieve a 12 % air void content, it was referred to as "CEI_{12}".

3. Results and analysis

3.1. Effect of particle-size sensor geometry

As an example, Fig. 6 shows the measured and global Euler angles for a representative specimen of the binder mixture compacted using Compactor 1 (gyrations between 50 and 55). It is worth noting that, in all plots, the secondary axis (Euler angles in the z direction) has a different scale with respect to the main axis (Euler angles in the x and y directions). In fact, for both sensors, the Euler angles in the z direction show a sawtooth trend with a steady decrease from + 180° to −180° that repeats cyclically every 2 s. This behaviour is related to the rotation of the entire system around its inclined axis in the case of Compactor 1 (see Fig. 2). More specifically, for this compactor, the sensor data denote a constant angular velocity related to the z axis of −180°/s (AsZ in Fig. 7), which corresponds to the mould rotation speed of 30 rpm.

For both sensors, the Euler angles in the x and y directions present a cyclic trend, with a period corresponding to the duration of one gyration (i.e., 2 s). For a given shell geometry, the amplitude of the sinusoids in the x and y directions is comparable. However, the comparison of the two geometries highlights that the measured Euler angles related to spherical sensor (Fig. 6(b)) are one order of magnitude larger than those measured with the cubic sensor (Fig. 6(a)). In addition, Fig. 6(a) shows that the amplitude of the sinusoids in the x and y directions remains quite stable for the cubic sensor, whereas it varies for the spherical sensor (Fig. 6(b)). Figs. 6(c) and 6(d) show the same Euler angles transformed into the global coordinate system during post-processing phase. Since the alignment to the global coordinates was already performed before starting the tests (auto-calibration), the measured Euler angles and the Euler angles referred to the global system differ slightly. These preliminary observations indicate that the spherical sensor moves significantly more than the cubic one during compaction.

Fig. 8 shows the relative rotations at horizontal directions (global coordinate system) obtained from the spherical and cubic sensors for a representative specimen of each mixture (Compactor 1 data). Consistently with what observed in Fig. 6 in terms of Euler angles, in all cases the RR values obtained from the spherical sensor are about ten times greater than those obtained from the cubic sensor. Additionally, it is important to note that the data related to the cubic sensor aligns with previous studies using the same geometry [8,9,11,12,14], even though the compaction mechanism of Compactor 1 may differ compared to the compactors used in the cited studies. The tenfold increase in x- and y-axis rotations observed for the spherical sensor compared to the cubic one may be explained by considering the overall behaviour of the sensors. During compaction, specimen height decreases by about 40 mm, resulting in a vertical displacement of approximately 20 mm for a sensor positioned at mid-height. The sensors do not directly register this

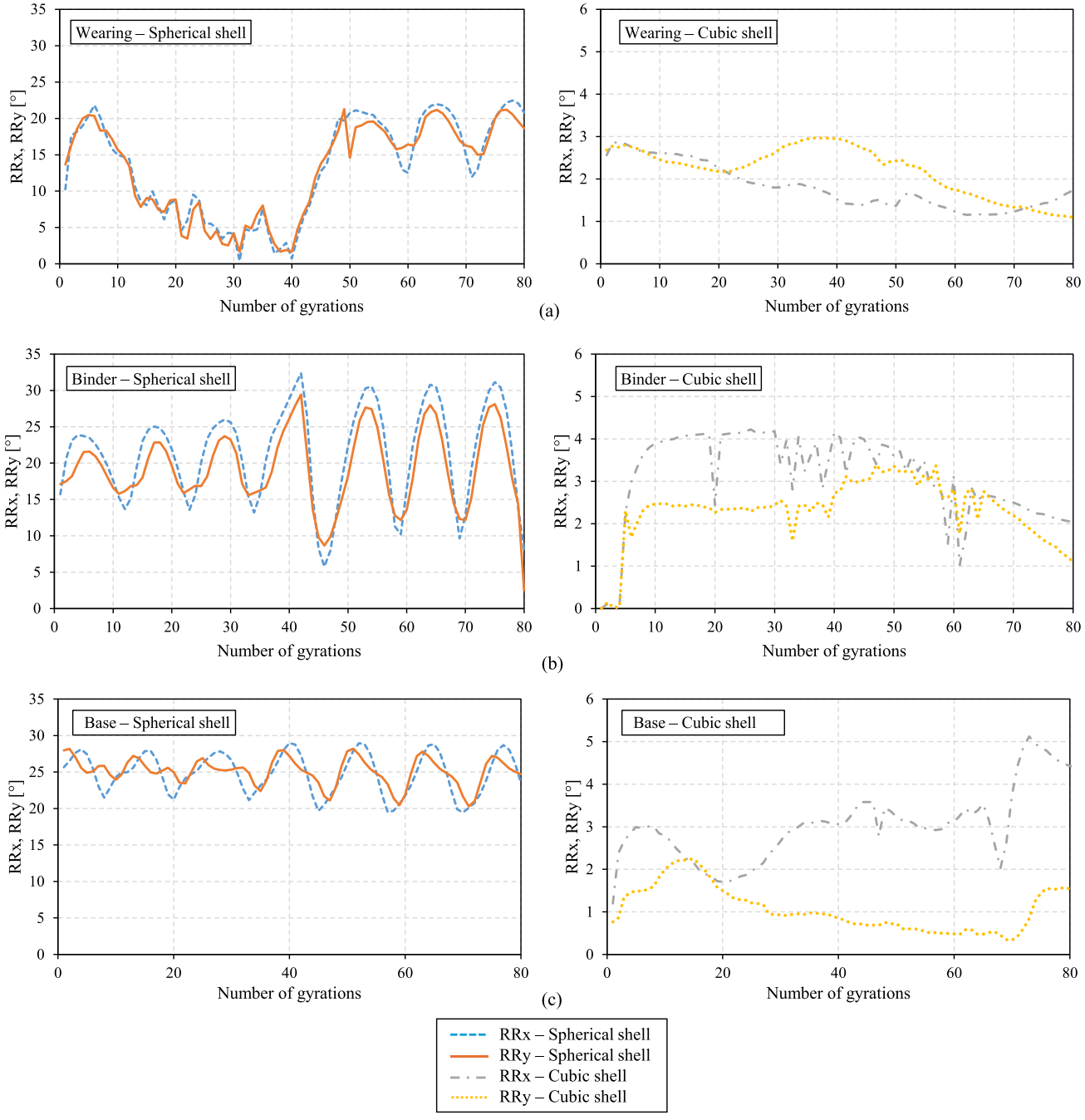

Fig. 8. Relative Rotations: (a) wearing, (b) binder, (c) base.

vertical displacement; instead, the spherical one records rotations on the plane normal to the compaction axis of about ±10°. This rotation amplitude corresponds to relative displacements along the mould axis of roughly ±3 mm at the sensor equator, which is consistent with the internal rearrangement of the mixture. In contrast, the cubic sensor, despite experiencing a similar vertical displacement, measures rotations limited to 1–2°, corresponding to relative axial displacements of about ±0.5 mm. This behaviour is likely due to its flat faces constraining free rotation. Furthermore, significant differences can be observed in the curve shapes for the two shells. The relative rotation curves derived from the spherical shell exhibit a cyclic pattern, whereas those derived from the cubic one show a generally decreasing trend without any cyclic pattern. These results are a consequence of the behaviour observed in Fig. 6 (constant amplitude vs. varying amplitude of the Euler angles in the x and y directions for the cubic sensor and spherical sensor, respectively).

Fig. 9(a) displays the RRC values at horizontal directions, confirming that the spherical sensor rotates significantly more than the cubic one when the same asphalt mixture is considered. This suggests that the spherical shell better follows the movement of the coarse aggregates during compaction, whereas, for the cubic shell, the confining action of the surrounding aggregates appears to be more pronounced, probably due to its large flat faces. Consequently, the low RR values measured using the cubic sensor may be due primarily to its shape. Therefore, it is expected that the spherical sensor can better distinguish between mixtures with good workability and mixtures with poor workability thanks to its greater freedom of movement.

The analysis of the air void content and CEI_{12} of the specimens

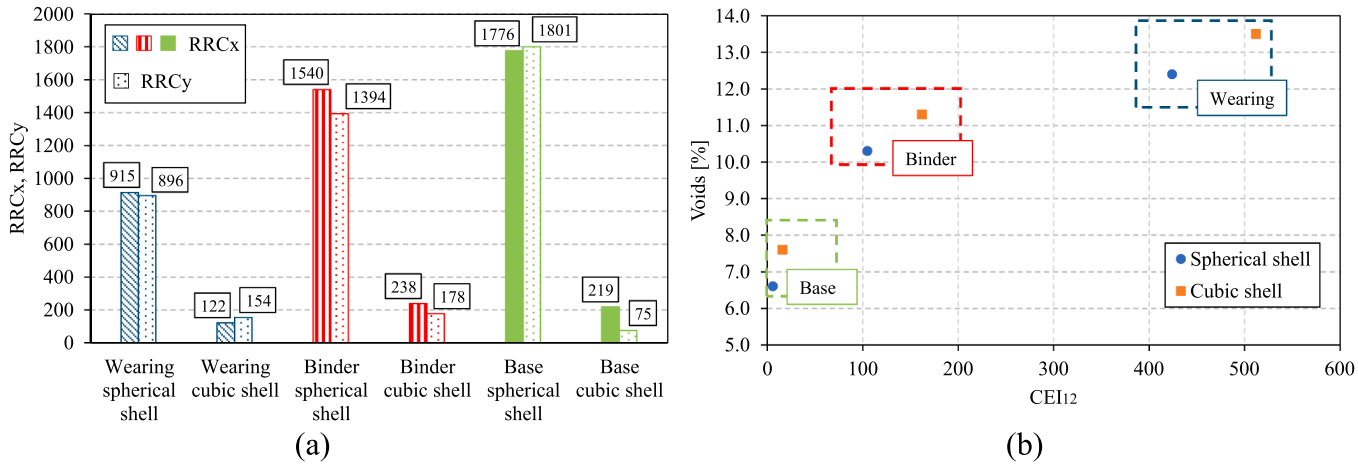

Fig. 9. Workability parameters: (a) Relative Rotation Capacity, (b) CEI_{12} and air void content.

Table 5
Average Residual Rotation values: effect of the sensor geometry.

Control Shell	Test Shell	Average Residual Rotation (ARR)					
		Wearing		Binder		Base	
		X direction	Y direction	X direction	Y direction	X direction	Y direction
Cubic	Spherical	112	105	182	170	219	243

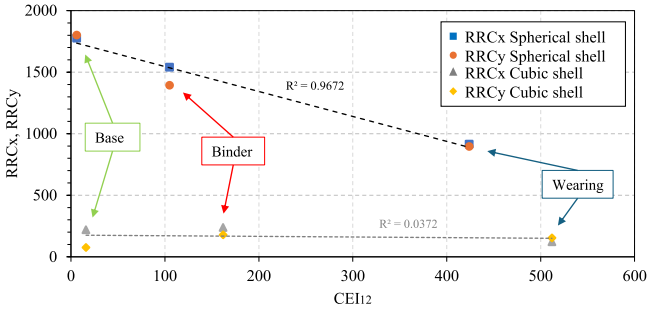

Fig. 10. Relative Rotation Capacity vs. CEI_{12}.

Table 6
Average Residual Rotation values: effect of the asphalt mixture type.

Control Mix	Test Mix	Average Residual Rotation (ARR)			
		Spherical shell		Cubic shell	
		X direction	Y direction	X direction	Y direction
Wearing	Binder	86	68	16	3
Wearing	Base	120	126	14	-11

compacted with different sensors also reveals some differences (Fig. 9 (b)). It should be noted that these parameters refer to the gyratory specimen as a whole, whereas the RRC values provided in Fig. 9(a) are derived from the data measured locally by the sensor. Fig. 9(b) shows that the air void content in the presence of the cubic sensor is approximately 1 % higher than that of specimens compacted with the spherical sensor. Analogously, in terms of energy required to achieve the same level of compaction, the CEI_{12} values are always higher (worse workability) for the cubic sensor as compared to the spherical sensor for a given asphalt mixture (Fig. 9(b)). Therefore, it appears that the cubic sensor may hinder the compaction process in the surrounding volume by obstructing the movement of the adjacent aggregates, although this could not be verified in the present study. Future work could investigate this aspect in more detail using methods such as X-ray computed tomography.

The average residual rotation (ARR) values, calculated considering the cubic shell and the spherical shell as the control and test shell respectively, also confirm this finding. The ARR values range from 100 in the case of the wearing course mixture to almost 250 in the case of the base mixture (Table 5), further highlighting that the spherical sensor rotates more than the cubic one during the compaction process.

It is noteworthy that, when using the spherical sensor, the RRC values are perfectly consistent with the air void content and CEI_{12} values. In this case, as depicted in Fig. 10, an increase in the RRC value corresponds to a decrease in the CEI_{12} value, which denotes better workability. Conversely, in the case of the cubic sensor, Fig. 10 shows that there is no clear relation between RRC and compaction energy (CEI_{12} index).

Therefore, among the reproducible sensor geometries considered in this study, the spherical one should be preferred over the cubic one. These findings are particularly relevant, considering that most studies employ cubic sensors or sensors with an irregular shape, and could also justify a revision of the ASTM D8541 standard in terms of sensor geometry.

3.2. *Effect of asphalt mixture type*

The results presented in Fig. 9 suggest that, among the studied mixtures, the wearing course mixture has the worst workability, as denoted by low RRC and high CEI_{12} and air void content values. Conversely, the base mixture presents the highest RRC values and the lowest CEI_{12} and air void content, suggesting that its workability is better than that of the other two mixtures. These results can be mainly attributed to the aggregate gradation and NMAS of the mixtures. However, the influence of the ratio between sensor size and mixture NMAS cannot be excluded. In fact, for the wearing course mixture, the aggregates may not be able to induce a significant movement of the sensor, whose presence may also alter the compaction process.

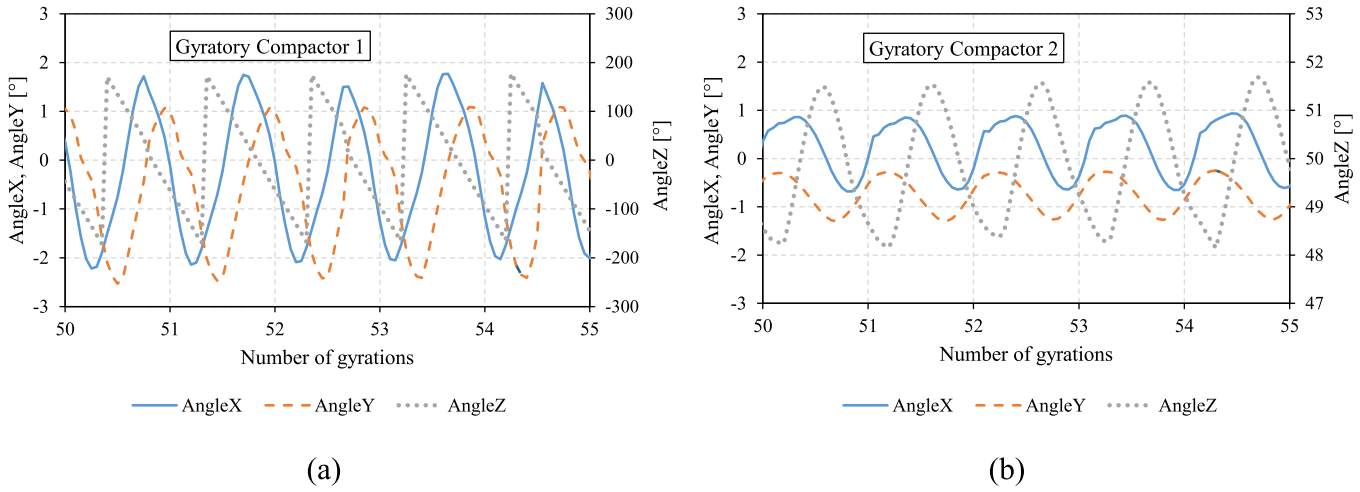

Fig. 11. Euler angles measured by the cubic sensor for the binder mixture: (a) Compactor 1, (b) Compactor 2.

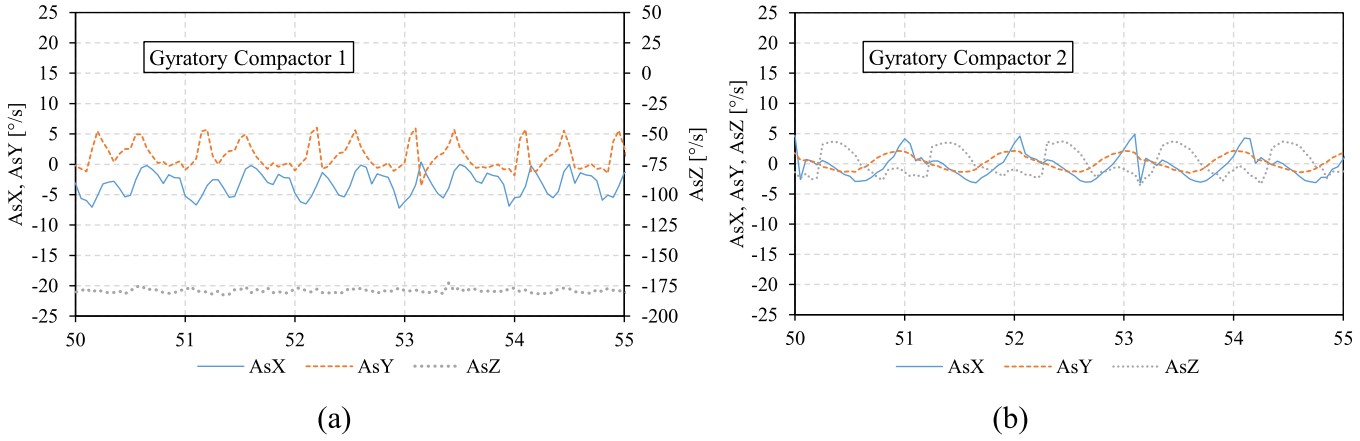

Fig. 12. Angular velocity measured by the cubic sensor for the binder mixture: (a) Compactor 1, (b) Compactor 2.

Table 7
Workability parameters for Compactor 1 and Compactor 2.

Mixture/ Shell	Gyratory Compactor	Air voids [%]	RRCx	RRCy	CEI_{12}
Binder/ Cubic shell	1	11.3	238	178	162
	2	10.8	128	78	117

To better compare the three asphalt mixtures, Table 6 shows the ARR values calculated by taking the wearing course mixture as the control mix. If the spherical sensor is considered, the data indicate that both the binder and the base mixtures have better workability than wearing course mixture (positive ARR values), with the highest ARR values observed for the base mixture. Instead, in the case of the cubic sensor, the absolute ARR values are low, and a negative ARR value is also observed in the y direction when comparing the wearing course mixture (control mix) with the base mixture (test mix). These findings further confirm that the low relative rotations experienced by the cubic sensor during the compaction may not allow to discriminate asphalt mixtures with different workability.

3.3. Effect of the gyratory compactor

The cubic sensor measurements were also used to compare the compaction mechanisms of the two gyratory compactors. Fig. 11 shows the measured Euler angles for the two compactors considering a representative specimen of the binder mixture. Similarly to Fig. 6, the Euler angles in the z direction are reported on the secondary axis, with a different scale.

It can be observed that, for Compactor 2, the measured Euler angles in the three directions all present a cyclic trend with comparable amplitudes (a few degrees). For Compactor 1, the Euler angles in the x and y directions show a cyclic evolution with amplitudes comparable to Compactor 2, whereas the Euler angles in the z direction are characterized by the previously highlighted sawtooth trend with values between $-180°$ and $+180°$, which is due to the rotation of the entire system around its inclined axis (Section 3.1). Fig. 12 shows the angular velocity measured in three directions by the cubic sensor for the binder mixture in the case of Compactor 1 (Fig. 12(a)) and Compactor 2 (Fig. 12 (b)). As already observed in Fig. 7, the angular velocity related to the z axis (AsZ) is constant and equal to $-180°/s$ for Compactor 1 (mould rotation speed of 30 rpm). On the contrary, for Compactor 2, the values of the angular velocity related to the z axis are comparable to those observed in the x and y directions (thus, the three angular velocities are represented on the same axis in Fig. 12(b)).

The workability parameters obtained for the two gyratory compactors are summarized in Table 7. It can be observed that the air void content at the end of the compaction process is basically the same (11.3 % for Compactor 1 vs. 10.8 % for Compactor 2). However, the

RRC values at horizontal directions and the CEI_{12} value are higher for Compactor 1, suggesting a possible influence of the compaction mechanism. Additional tests employing the spherical sensor are already planned in order to draw a solid conclusion on this aspect.

4. Conclusions

The objective of this study was to compare particle-size sensors of different geometry, in order to verify their behaviour during compaction and their ability to analyse the workability parameters of asphalt mixtures. To this aim, two easily reproducible sensor geometries (cubic, spherical) and three asphalt mixtures with different characteristics (e.g., NMAS) were investigated in the laboratory. Moreover, the study employed two gyratory compactors with different compaction mechanisms to provide a preliminary analysis of the gyratory compactor influence.

The experimental results led to the following main conclusions:

- The particle-size sensor geometry affects its measurements: relative rotation values obtained from the spherical sensor are about ten times greater than those obtained from the cubic sensor. The spherical sensor better follows the movement of the aggregates during compaction, whereas the confining action of the surrounding aggregates appears to be more pronounced in the case of the cubic sensor because of its flat faces. Therefore, the spherical sensor may be more sensitive to workability variations. In addition, specimens compacted using the cubic sensor exhibit an air void content approximately 1 % greater than those compacted with the spherical sensor. Therefore, it can be deduced that the cubic sensor could hinder the compaction process in the surrounding mixture volume by impeding the movement of the adjacent aggregates (this aspect could be validated in future studies using methods such as X-ray computed tomography). These findings could lay the foundations for a revision of the reference ASTM D8541 standard in terms of sensor geometry.
- The spherical sensor made it possible to observe significant differences between the three asphalt mixtures, which can be mainly attributed to the different NMAS and gradation of the mixtures. The base mixture exhibits RRC values twice as high as those of the wearing mixture in the case of spherical shell, while its CEI values are ten times lower. However, the potential influence of the ratio between sensor size and mixture NMAS cannot be entirely excluded. Therefore, further tests are necessary to verify this point.
- The different compaction mechanism of the gyratory compactors used had a measurable influence on the workability parameters. However, additional tests with the spherical sensor are needed to draw definitive conclusions on this aspect.

In conclusion, particle-size sensors can provide a direct, real-time measurement of internal mixture rearrangements during compaction, complementing conventional bulk indicators such as density or CEI. Selecting the appropriate sensor geometry may play a crucial role in assessing workability parameters (such as RR, RRC, ARR), thereby guiding the optimisation of mix design during laboratory testing.

Future studies will evaluate the effects of the compaction temperature and the use of warm mix asphalt technologies, the laboratory compaction with the roller compactor, and the possible field application of the developed particle-size sensors.

CRediT authorship contribution statement

Andrea Graziani: Writing – review & editing, Methodology, Formal analysis, Conceptualization. **Francesco Canestrari:** Writing – review & editing, Methodology, Formal analysis, Conceptualization. **Amedeo Virgili:** Writing – review & editing, Software, Methodology, Formal analysis. **Omar Guazzaroni:** Writing – original draft, Methodology, Investigation, Formal analysis. **Lorenzo Paolo Ingrassia:** Writing – original draft, Methodology, Formal analysis, Conceptualization.

Declaration of Competing Interest

The authors declare that they have no known competing financial interests or personal relationships that could have appeared to influence the work reported in this paper.

Data availability

Data will be made available on request.

References

[1] F. Pérez-Jiménez, A.H. Martínez, R. Miró, D. Hernández-Barrera, L. Araya-Zamorano, Effect of compaction temperature and procedure on the design of asphalt mixtures using Marshall and gyratory compactors, Constr. Build. Mater. 65 (2014) 264–269.
[2] H.M. Radzi, R. Muniandy, S. Hassim, T.H. Law, F.M. Jakarni, An overview of asphalt mix designs using various compactors, IOP Conference Series Materials Science Engineering 512 (1) (2019) 01203.
[3] X. Wang, S. Shen, H. Huang, L.C. Almeida, Characterization of particle movement in Superpave gyratory compactor at meso-scale using SmartRock sensors, Constr. Build. Mater. 175 (2018) 206–214.
[4] S. Liu, H. Huang, T. Qiu, L. Gao, Comparison of laboratory testing using smartrock and discrete element modeling of ballast particle movement, J. Mater. Civ. Eng. 29 (3) (2017) D6016001.
[5] S. Liu, H. Huang, T. Qiu, J. Kwon, Effect of geogrid on railroad ballast particle movement, Transp. Geotech. 9 (2016) 110–122.
[6] ASTM D8541, 2024. Standard Test Method for Determination of Relative Rotation to Evaluate the Workability of Asphalt Mixture Using Wireless Particle-Size Sensors.
[7] H.-C. Dan, D. Yang, L.-H. Zhao, S.-P. Wang, Z. Zhang, Meso-scale study on compaction characteristics of asphalt mixtures in Superpave gyratory compaction using SmartRock sensors, Constr. Build. Mater. 262 (2020) 120874.
[8] S. Yu, S. Shen, R. Steger, X. Wang, Effect of warm mix asphalt additive on the workability of asphalt mixture: From particle perspective, Constr. Build. Mater. 360 (2022) 129548.
[9] R. Ma, Z. Wang, Study on the compaction performance and its key influencing factors of asphalt mixture based on intelligent sensing techniques, J. Sens. 2023 (2023) 2224322.
[10] X. Wang, H. Huang, E. Tutumluer, J.S. Tingle, S. Shen, Monitoring particle movement under compaction using smartrock sensor: a case study of granular base layer compaction, Transp. Geotech. 34 (2022) 100764.
[11] Y. Xiao, M. Wang, X. Wang, J. Ren, W. Wang, X. Chen, Evaluating gyratory compaction characteristics of unbound permeable aggregate base materials from meso-scale particle movement measured by smart sensing technology, Materials 14 (15) (2021) 4287.
[12] N. Wang, F. Chen, T. Ma, Y. Luan, J. Zhu, Compaction performance of cold recycled asphalt mixture using SmartRock sensor, Autom. Constr. 140 (2022) 104377.
[13] X. Wang, S. Shen, H. Huang, Z. Zhang, Towards smart compaction: particle movement characteristics from laboratory to the field, Constr. Build. Mater. 218 (2019) 323–332.
[14] X. Wang, S. Shen, H. Huang, Meso-scale kinematic responses of asphalt mixture in both field and laboratory compaction, Transp. Res. Rec. 2675 (9) (2021) 1631–1642.
[15] H.C. Dan, D. Yang, X. Liu, A.P. Peng, Z. Zhang, Experimental investigation on dynamic response of asphalt pavement using SmartRock sensor under vibrating compaction loading, Constr. Build. Mater. 247 (2020) 118592.
[16] H.C. Dan, Z. Zhang, H. Shan, W. Cao, Preliminary characterization on the dynamic mechanism of asphalt mixture under on-site vibratory compaction, Constr. Build. Mater. 400 (2023) 132695.
[17] Z. Zhang, H. Dan, S. Li, W. Li, Optimizing asphalt surface course compaction: insights from aggregate triaxial acceleration responses, Materials 16 (22) (2023) 7239.
[18] T. Ma, N. Wang, C. Han, S. Wang, Z. Tong, Asphalt pavement residual life assessment based on smartrock sensors, IEEE Trans. Instrum. Meas. 72 (2023) 9505912.
[19] C. Zhang, D.G. Ildefonzo, S. Shen, L. Wang, H. Huang, Implementation of ensemble Artificial Neural Network and MEMS wireless sensors for In-Situ asphalt mixture dynamic modulus prediction, Constr. Build. Mater. 377 (2023) 131118.
[20] X. Ding, F. Liu, F. Huang, T. Ma, J. Zhang, Micro-scale investigation on aggregate skeleton behavior of asphalt mixture: Mechanism and monitoring, Constr. Build. Mater. 437 (2024) 137062.
[21] N. Wang, T. Han, H. Cheng, T. Li, J. Fu, T. Ma, Y. Fu, F. Chen, Y. Zhang, Monitoring structural health status of asphalt pavement using intelligent sensing technology, Constr. Build. Mater. 352 (2022) 129025.
[22] Y. Li, W. Jiang, J. Xiao, F. Zhao, S. Zhang, C. Xing, D. Yuan, Effects of kneading and impact action on the movement of aggregates in asphalt mixtures during compaction, Constr. Build. Mater. 366 (2023) 130210.

[23] S. Komaragiri, A. Gigliotti, A. Bhasin, Feasibility of using a physics engine to virtually compact asphalt mixtures in a gyratory compactor, Constr. Build. Mater. 308 (2021) 124977.
[24] S. Yu, S. Shen, Compaction prediction for asphalt mixtures using wireless sensor and machine learning algorithms, IEEE Trans. Intell. Transp. Syst. 24 (1) (2023) 778–786.
[25] D. Zhang, Z. Cheng, D. Geng, S. Xie, T. Wang, Experimental and numerical analysis on mesoscale mechanical behavior of coarse aggregates in the asphalt mixture during gyratory compaction, Processes 10 (1) (2022) 47.
[26] Y. Li, C. Mao, M. Sun, J. Hong, X. Zhao, P. Li, J. Xiao, Effect of smart aggregate size on mesostructure and mechanical properties of asphalt mixtures, Coatings 14 (10) (2024) 1238.
[27] EN 12697-31:2019, Bituminous mixtures – Test methods – Part 31: Specimen preparation by gyratory compactor.
[28] Guazzaroni O., Binni L., D'Aparo R., Graziani A., Ingrassia L.P., Naticchia B., Virgili A., Canestrari F., 2025. Workability evaluation of asphalt mixtures using SmartRock sensors: effect of shell shape. Presented during the "3rd International Symposium on Pavement Functional Design and Management", Delft (The Netherlands), 2-4 July 2025.
[29] EN 12697-8:2019, Bituminous mixtures – Test methods – Part 8: Determination of void characteristics of bituminous specimens.
[30] EN 12697-6:2020, Bituminous mixtures – Test methods – Part 6: Determination of bulk density of bituminous specimens.
[31] A.F.F. Mahmoud, H.U. Bahia, Using the gyratory compactor to measure mechanical stability of asphalt mixtures. Report WHRP 05-02, University of Wisconsin, Madison, 2004.
[32] X. Wang, S. Shen, H. Huang, S. Yu, Understanding the role of particle rotation in asphalt mixture compaction by tracking coarse aggregate movement, Constr. Build. Mater. 395 (2023) 132325.